Modelling Axisymmetric Centrifugal Compressor Characteristics from First Principles

Katherine H. Powers
Dept. of Mathematical Sciences
University of Bath
Claverton Down, Bath, BA2 7AY
United Kingdom
Email: k.h.powers@bath.ac.uk

Chris J. Brace
Dept. of Mechanical Engineering
University of Bath
Claverton Down, Bath, BA2 7AY
United Kingdom
Email: c.j.brace@bath.ac.uk

Chris J. Budd
Dept. of Mathematical Sciences
University of Bath
Claverton Down, Bath, BA2 7AY
United Kingdom
Email: c.j.budd@bath.ac.uk

Colin D. Copeland
School of
Sustainable Energy Engineering
Simon Fraser University
University Drive, Surrey, V3T 0N1
BC, Canada
Email: ccopelan@sfu.ca

Paul A. Milewski
Dept. of Mathematical Sciences
University of Bath
Claverton Down, Bath, BA2 7AY
United Kingdom
Email: p.a.milewski@bath.ac.uk

ABSTRACT

Turbochargers are a vital component for aiding engine manufacturers in meeting the latest emissions standards. However, their range of operation is limited for low mass flows by compressor surge. Operation in surge results in pressure and mass flow oscillations that are often damaging to the compressor and its installation. Since surge is a highly complex flow regime, full unsteady 3D models are generally too computationally expensive to run. The majority of current low-dimensional surge models use a cubic compressor characteristic that needs to be fitted to experimental data. Therefore, each time a compressor is studied using these models, costly experimental testing is required.

In this paper, a new technique for obtaining an axisymmetric centrifugal compressor characteristic is presented. This characteristic is built using the equations of mass, momentum and energy from first principles in order to provide a more complete model than those currently obtained via experimental data. This approach enables us to explain the resulting cubic-like shape of the characteristic and hence to identify impeller inlet stall as a route into surge. The characteristic is used within a quasi-steady, map-based surge model in order to demonstrate its ability to predict the onset of surge while only providing geometric data as input. Validation is provided for this model by discussion of the qualitative flow dynamics and a good fit to experimental data, especially for low impeller speeds and pressure ratios.

INTRODUCTION

There are a huge number of applications for centrifugal compressors [1]. Although the methodology presented in this paper is applicable to all centrifugal compressors (via the extension of models by, for example, Macdougal et al. [2] who developed a 1D map-based model for process plant applications), we will focus on the application to turbocharger compressors for the automotive industry.

Turbocharger compressors are normally used to increase the power output of smaller engines so they can be used in place of larger naturally aspirated ones, making the vehicle more environmentally friendly [3]. They need a wide stable operating range, but this range is limited by surge at low mass flow rates and choke at high mass flow rates.

Surge is an instability that results in audible mass flow and pressure oscillations that would be off-putting to any driver. Moreover, these oscillations, in combination with an increase in temperature, often damage the compressor or its installation.

Surge is commonly found to be triggered by some form of stall. There are two main types of stall. The first can occur at the inlet to the impeller or a vaned diffuser and is caused by incidence. This means that, as mass flow decreases, the inlet flow angle increases and causes a separation of the flow at the blade or vane wall [4]. In the impeller this stall can pass between neighbouring channels to become a rotating stall. The second type is often seen in a vaneless diffuser and is caused by recirculation. This is where friction reduces the radial velocity of the flow near the shroud-side wall of the diffuser, reducing its spiral angle so that it is swept back into the impeller [4].

The stalling of the impeller and diffuser can occur individually or simultaneously, but are not independent as stall in one component influences the behaviour of stall in the other. There is extensive literature on the

stall and surge behaviour of compressors, for example [5–9].

Since surge limits the amount of boost provided at low engine speeds, there is a desire to operate close to surge without entering it for prolonged periods of time. Therefore, it becomes essential to create models that can predict the location of the surge region, as well as aid understanding of the flow dynamics near that region.

A very common numerical modelling approach is Computational Fluid Dynamics (CFD). In a CFD model, a 3D domain is built in the computer and a mesh is inserted into it. This mesh divides the domain into millions of control volumes, or cells, within which the conservation of mass, momentum and energy equations can be solved numerically [10]. The accuracy of CFD computations has increased dramatically over the past decades due to the rapid growth in high speed computing power. However, CFD can struggle when modelling large scale phenomena that depend on small scale effects because it is too computationally expensive to perform this direct numerical simulation with the required fineness of mesh [10]. Since surge cycles often experience local or small scale phenomena like rotating stall, recirculation and eddies, full unsteady 3D CFD is required to completely capture the dynamics. However, the computational cost of this is not suitable for industrial needs [11].

Map based models provide a popular alternative to CFD for modelling surge. All of these models take as an input a compressor map that has been extended beyond the surge point and into reversed flows. The speed lines on these extended compressor maps are often referred to as compressor characteristics.

Usually these models assume that at any given time the compressor is operating in steady-state, and so are quasi-steady in nature. There are many examples of these models in the literature for various compressor types and applications [6, 12–15]. However, there has been some work on unsteady 1D models that incorporate the compressor map as a boundary condition [16, 17].

The majority of these models are based on a nonlinear model by Greitzer in 1976 [18]. Greitzer modelled an axial compression system by use of two actuator disks, one to represent the compressor and the other to represent the throttle valve. These are connected together by a pipe and a large plenum. The flow is considered incompressible within the pipe and to have negligible kinetic energy within the plenum. This generates a set of ODEs to model the behaviour of flow in the compression system, for example the

Moore-Greitzer model [18, 19]

$$\frac{d\Phi}{dt} = B(\psi_c - \Psi) \tag{1}$$

$$\frac{d\Psi}{dt} = \frac{1}{B}(\Phi - \psi_T^{-1}) \tag{2}$$

for nondimensional mass flow, Φ, and pressure, Ψ, where ψ_c and ψ_T are compressor and throttle characteristics respectively.

For the throttle characteristic ψ_T, the Orifice Equation [19],

$$\psi_T = \xi_{T0} + \frac{1}{\xi_T^2}\Phi^2, \tag{3}$$

is typically used.

There have been three main approaches for obtaining the compressor characteristics. The first is through complex experimental studies, for example, Koff and Greitzer in 1984 [20] proposed a cubic-like shape after experimentally testing an axial compressor in various flow regimes. The curve was reasonably straightforward to determine in backflow and steady forward flow regimes. However, when rotating stall appeared the shape was more difficult to determine, and so transients were analysed and an argument was made for having a smoothly varying characteristic based on the behaviour of diffuser stall. This has been done more recently for small centrifugal compressors by Galindo et al. [21], also producing a cubic-like curve.

The second approach is via curve fitting and extrapolation. The most common technique is to use the cubic relation proposed by Moore and Greitzer in 1986 [22], i.e.

$$\psi_c = \psi_{c_0} + H\left[1 + \frac{2}{3}\left(\frac{\Phi}{W} - 1\right) - \frac{1}{2}\left(\frac{\Phi}{W} - 1\right)^3\right] \tag{4}$$

with parameters H and W found through fitting to experimental compressor map data. However other curve fitting techniques have been proposed, including ones involving Chebyshev polynomials in order to capture more features of the characteristics [23], and ones involving elliptic equations in order to adjust the

characteristic for different settings on a variable-geometry diffuser [24].

The third is via mean-line modelling. In a mean-line model the compressor is divided into sections over which the equations of motion and loss models are evaluated. Most of the mean-line models follow the meridional path of the compressor and typically split it into sections for the inlet, impeller, diffuser and volute [25, 26]. However, there are two-zone models that have primary and secondary flow sections within the impeller in order to account for slip [27]. The majority of these mean-line models apply empirical loss models to the sections. Typical collections of loss models for compressors can be found in [28–30]. These loss models usually have loss coefficients that need to be tuned to the particular compressor that is being studied, which makes mean-line modelling still partially reliant on data or CFD simulation.

The advantage of the purely experimental approach for finding compressor characteristics is its simplicity because reading data or evaluating polynomial-like expressions is very quick computationally. However, map-based surge models are sensitive to the shape of the compressor characteristic, so it is vital to understand this fully, and an experimental approach doesn't give us any insight into the reason why we get this shape of curve. In addition, since surge is a system phenomenon, experimentally measured surge can be limited to the particular experimental set-up and not, as would be desirable, any compressor installation.

The mean-line model approach can provide some understanding of the characteristic's shape because it is based in part on the physical equations of motion, and a tuned mean-line model produces some good results. However, this model usually still requires compressor specific data to tune the loss coefficients. Ideally, we would like a model that works for every type of compressor using only known information, like geometry, therefore any parameters in the model need to be universal.

In this paper, compressor characteristics are generated through simulations of a physical model for the compressor. This physical model is derived from first principles and uses inputs solely from geometry. It has been designed to be as simple as possible while still capturing the dynamics of surge. Therefore, it contains a minimal number of parameters and has found relations for these that make them universally applicable. The strength of having a mathematically simple model is that it can be used for things like bifurcation analysis, which is a powerful tool to study the dynamics of surge as parameters, such as geometrical dimensions, are changed.

Since the model has been built from physical principles and is theoretical in nature, it gives us new understanding of the stall and surge phenomena, which in turn will help in the design of future compressors. To the authors' knowledge, this is the first time that such a model has been created, and it makes an important step in updating the low-dimensional surge models that have remained relatively unchanged over

the past 30 years. This novel approach will enable low-dimensional surge models to be a useful tool for turbocharger designers, as it will provide insight into the surge limitations of a new design while reducing the need for testing during preliminary design stages.

EQUATIONS OF MOTION

The key physical laws needed for deriving a model for a compressor from first principles are conservation of mass,

$$\frac{\partial \rho}{\partial t} + \nabla \cdot (\rho \mathbf{u}) = 0, \tag{5}$$

conservation of momentum in a rotating frame,

$$\frac{\partial}{\partial t}(\rho \mathbf{u}) + \nabla \cdot (\rho(\mathbf{u} \otimes \mathbf{u})) + 2\rho(\mathbf{\Omega} \times \mathbf{u}) + \rho(\mathbf{\Omega} \times (\mathbf{\Omega} \times \mathbf{r})) = \rho \mathbf{g} - \nabla p + \nabla \cdot \tau, \tag{6}$$

and conservation of energy,

$$\frac{\partial}{\partial t}(\rho E) + \nabla \cdot (\rho \mathbf{u} E + p\mathbf{u}) - \nabla \cdot (\tau \cdot \mathbf{u}) = \rho \dot{Q}. \tag{7}$$

In the inertial frame of reference,

$$E = \frac{|\mathbf{u}|^2}{2} + U, \tag{8}$$

where U is the specific internal energy. However, when we are in a rotating frame of reference, E becomes the relative specific energy, so

$$E + \frac{\Omega^2 r^2}{2} = \frac{|\mathbf{u}|^2}{2} + U, \tag{9}$$

to take into account the energy added to the flow by the rotation.

We also need the ideal gas law,

$$p = \rho R T, \tag{10}$$

and the assumption of a perfect gas so that

$$U = c_v T = \frac{1}{\gamma - 1}\frac{p}{\rho}, \tag{11}$$

where c_v and γ are assumed constant.

Since we are dealing with gases, it seems reasonable to assume gravitational and viscous effects are negligible, however, we will include a term, $\mathbf{F}$, in the momentum equation to account for frictional losses. We will also assume that the flow is adiabatic because the timescale of heat-transfer is much longer than that of the flow velocities associated with turbochargers. Finally, we are looking for a steady-state characteristic, so we will remove the time dependence.

MODEL DERIVATION

The main components in a compressor are the impeller and the diffuser. It is easiest to consider these separately so different simplifying assumptions can be made.

Impeller

Figure 1 shows a comparison of a typical impeller geometry to the impeller geometry we will assume in this model.

This simplified geometry allows us to assume that air flows through the compressor in a predominantly radial direction. Due to the straight radial blades, we can assume that $u_\theta = 0$ in the rotating frame of

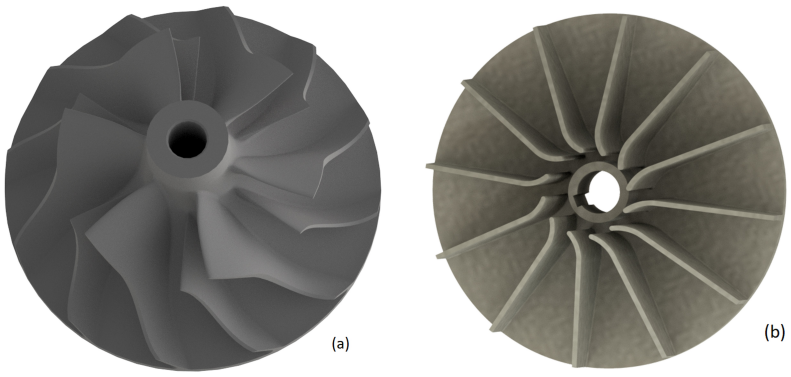

Fig. 1. (a) A TYPICAL IMPELLER FROM A CENTRIFUGAL COMPRESSOR. IT HAS BACKSWEPT BLADES AND TURNS THE FLOW FROM THE AXIAL DIRECTION TO THE RADIAL DIRECTION AS IT COMPRESSES. (b) THE SIMPLIFIED IMPELLER GEOMETRY USED IN THE MODEL DERIVATION. HERE THE FLOW TRAVELS RADIALLY FROM THE CENTRE OF THE IMPELLER TO THE OUTLET. IT HAS STRAIGHT RADIAL BLADES, BUT DOES HAVE AN INLET BLADE ANGLE SO THE MODEL CAN ACCOUNT FOR THE EFFECTS OF POOR INLET FLOW ALIGNMENT.

reference. Therefore, after writing in cylindrical polar coordinates, Eqns. 5-7 become

$$\frac{1}{r}\frac{\partial}{\partial r}(r\rho u_r) + \frac{\partial}{\partial x}(\rho u_x) = 0, \tag{12}$$

$$\frac{1}{r}\frac{\partial}{\partial r}(r\rho u_r^2) + \frac{\partial}{\partial x}(\rho u_r u_x) - \rho\Omega^2 r = -\frac{\partial p}{\partial r} + F_r, \tag{13}$$

$$2\rho\Omega u_r = -\frac{1}{r}\frac{\partial p}{\partial \theta} + F_\theta, \tag{14}$$

$$\frac{1}{r}\frac{\partial}{\partial r}(r\rho u_x u_r) + \frac{\partial}{\partial x}(\rho u_x^2) = -\frac{\partial p}{\partial x} + F_x, \tag{15}$$

$$\frac{1}{r}\frac{\partial}{\partial r}(r u_r(\rho E + p)) + \frac{\partial}{\partial x}(u_x(\rho E + p)) = 0. \tag{16}$$

where

$$E = \frac{u_r^2}{2} + \frac{u_x^2}{2} + \frac{1}{\gamma - 1}\frac{p}{\rho} - \frac{\Omega^2 r^2}{2}. \tag{17}$$

Defining the average of a quantity, G, by

$$\bar{G} = \frac{1}{h(r)} \int_0^{h(r)} G \; dx, \tag{18}$$

where h is the height of the impeller blade, and using the Leibniz rule for differentiation under the integral sign, we can average Eqns. 12, 13, and 16 to get

$$\frac{1}{r}\frac{\partial}{\partial r}(rh\overline{\rho u_r}) = 0, \tag{19}$$

$$\frac{1}{r}\frac{\partial}{\partial r}(rh\overline{\rho u_r^2}) - h\bar{\rho}\Omega^2 r = -\frac{\partial}{\partial r}(h\bar{p}) + p\Big|_h \frac{\partial h}{\partial r} + h\bar{F}_r, \tag{20}$$

$$\frac{1}{r}\frac{\partial}{\partial r}(rh\overline{\rho u_r E} + rh\overline{u_r p}) = 0, \tag{21}$$

subject to no-flux boundary conditions.

At this point, further assumptions are necessary. Firstly, we assume that we can approximate averaged products by $\overline{ab} = \bar{a}\bar{b}$, which requires one of the variables to not deviate much from its mean value. Secondly, we assume that

$$p\Big|_h = \bar{p}, \tag{22}$$

and, finally, we take $\bar{u}_x$ as small, so

$$\bar{E} = \frac{\bar{u}_r^2}{2} - \frac{\Omega^2 r^2}{2} + \frac{1}{\gamma - 1}\frac{\bar{p}}{\bar{\rho}}. \tag{23}$$

This means that a 1D model for the flow in the impeller is given by

$$\frac{1}{r}\frac{\partial}{\partial r}(rh\rho u_r) = 0, \tag{24}$$

$$\frac{1}{r}\frac{\partial}{\partial r}(rh\rho u_r^2) - h\rho\Omega^2 r = -h\frac{\partial p}{\partial r} + hF_r, \tag{25}$$

$$\frac{1}{r}\frac{\partial}{\partial r}\left(rh\rho u_r\left(\frac{u_r^2}{2} + \frac{\gamma}{\gamma-1}\frac{p}{\rho} - \frac{\Omega^2 r^2}{2}\right)\right) = 0, \tag{26}$$

where the bars have been dropped for convenience.

Diffuser

The diffuser is non-rotating, so $\Omega = 0$, and we return to the inertial frame of reference. It is also assumed that the compressor has a vaneless diffuser, which allows the assumption that all variables are independent of θ.

Therefore, in this case Eqns. 5-7 become

$$\frac{1}{r}\frac{\partial}{\partial r}(r\rho u_r) + \frac{\partial}{\partial x}(\rho u_x) = 0, \tag{27}$$

$$\frac{1}{r}\frac{\partial}{\partial r}(r\rho u_r^2) + \frac{\partial}{\partial x}(\rho u_r u_x) - \frac{\rho u_\theta^2}{r} = -\frac{\partial p}{\partial r} + F_r, \tag{28}$$

$$\frac{1}{r}\frac{\partial}{\partial r}(r\rho u_r u_\theta) + \frac{\partial}{\partial x}(\rho u_\theta u_x) + \frac{\rho u_r u_\theta}{r} = F_\theta, \tag{29}$$

$$\frac{1}{r}\frac{\partial}{\partial r}(r\rho u_x u_r) + \frac{\partial}{\partial x}(\rho u_x^2) = -\frac{\partial p}{\partial x} + F_x, \tag{30}$$

$$\frac{1}{r}\frac{\partial}{\partial r}(ru_r(\rho E + p)) + \frac{\partial}{\partial x}(u_x(\rho E + p)) = 0, \tag{31}$$

where

$$E = \frac{u_r^2}{2} + \frac{u_x^2}{2} + \frac{1}{\gamma-1}\frac{p}{\rho}. \tag{32}$$

Averaging Eqns. 27, 28, 29 and 31 subject to no-flux conditions as before, gives

$$\frac{1}{r}\frac{\partial}{\partial r}(rh\overline{\rho u_r}) = 0, \tag{33}$$

$$\frac{1}{r}\frac{\partial}{\partial r}(rh\overline{\rho u_r^2}) - \frac{h\overline{\rho u_\theta^2}}{r} = -h\frac{\partial \bar{p}}{\partial r} + h\bar{F}_r, \tag{34}$$

$$\frac{1}{r}\frac{\partial}{\partial r}(rh\overline{\rho u_r u_\theta}) + \frac{h\overline{\rho u_r u_\theta}}{r} = h\bar{F}_\theta, \tag{35}$$

$$\frac{1}{r}\frac{\partial}{\partial r}(rh\overline{\rho u_r E} + rh\overline{u_r p}) = 0. \tag{36}$$

Therefore, using the same assumptions as we did for the impeller, so that $\overline{ab} = \bar{a}\bar{b}$ and

$$\bar{E} = \frac{\bar{u}_r^2}{2} + \frac{\bar{u}_\theta^2}{2} + \frac{1}{\gamma - 1}\frac{\bar{p}}{\bar{\rho}}, \tag{37}$$

we get the following system of equations for the diffuser (after dropping the bars):

$$\frac{1}{r}\frac{\partial}{\partial r}(rh\rho u_r) = 0, \tag{38}$$

$$\frac{1}{r}\frac{\partial}{\partial r}(rh\rho u_r^2) - \frac{h\rho u_\theta^2}{r} = -h\frac{\partial p}{\partial r} + hF_r, \tag{39}$$

$$\frac{1}{r}\frac{\partial}{\partial r}(rh\rho u_r u_\theta) + \frac{h\rho u_r u_\theta}{r} = hF_\theta, \tag{40}$$

$$\frac{1}{r}\frac{\partial}{\partial r}\left(rh\rho u_r\left(\frac{u_r^2}{2} + \frac{u_\theta^2}{2} + \frac{\gamma}{\gamma - 1}\frac{p}{\rho}\right)\right) = 0. \tag{41}$$

Friction

Skin friction is the only type of frictional loss that is considered in this model. It is defined as the shear stress exerted by the fluid on the surface over which it flows [31]. Therefore, if τ_w denotes the wall shear stress,

$$F = -\tau_w S \tag{42}$$

$$\implies F = -\frac{1}{2} f \rho u_r^2 S \tag{43}$$

where S denotes the total surface area of the contact faces between the walls and the fluid per unit volume, and

$$f = \frac{\tau_w}{\frac{1}{2}\rho u_r^2} \tag{44}$$

is the Fanning friction factor [32].

Therefore, in the impeller we have

$$F_r = -\frac{1}{2} f \rho u_r^2 S_I, \tag{45}$$

where

$$S_I = 2\left(\frac{n_b}{2\pi r} + \frac{1}{h}\right), \tag{46}$$

and for the diffuser we have

$$F_r = -\frac{1}{2} f \rho u_r^2 S_D, \tag{47}$$

$$F_\theta = -\frac{1}{2} f \rho u_r u_\theta S_D, \tag{48}$$

where

$$S_D = \frac{2}{h}. \tag{49}$$

Stalling

The mass flow rate is defined as $\dot{m} = A\rho u_r$ for a cross-sectional area A. In the diffuser the area is simply $A = 2\pi r h$. However, in the impeller we can get stalling at the inlet. As seen in Fig. 2, low inlet

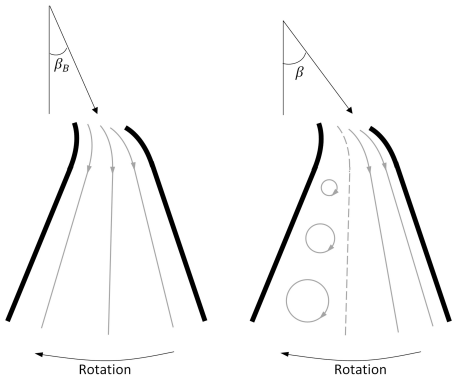

Fig. 2. IMPELLER CHANNELS IN UNSTALLED (LEFT) AND STALLED (RIGHT) CONDITIONS. THE STALLED CHANNEL IS CAUSED BY A LOW INLET RADIAL VELOCITY THAT LEADS TO A LARGE INLET FLOW ANGLE β IN COMPARISON TO THE BLADE ANGLE β_B. THE UNSTALLED CHANNEL IS SHOWN WITH AN INLET FLOW ANGLE THAT MATCHES THE BLADE ANGLE β_B PERFECTLY.

velocities lead to large flow angles, β, which result in flow separation. This region of stalled flow effectively blocks part of the channel, and so reduces the area of the channel available to the unstalled flow.

Therefore, defining the impeller area as $A = \theta r h$ for

$$\theta = \begin{cases} \frac{2\pi}{\left(1+\alpha\left(1-\frac{\tan\beta_B}{\tan\beta}\right)^2\right)} & \beta > \beta_B \\ 2\pi & \text{otherwise} \end{cases} \tag{50}$$

where β_B is the inlet blade angle of the impeller, allows us to take into account this stalling. The parameter α is used to control the strength of the stalling, for example, if A_0 is the area of the entire channel, then the maximum blockage results in an area of $\frac{1}{1+\alpha}A_0$.

It is not uncommon to use blockage as a way to represent stalled flow regimes. Day et al. [33] developed a model for rotating stall in an axial compressor. They noted that stall cells had negligible axial velocity whereas the unstalled regions had a higher axial velocity than expected. This led to them including a stall cell blockage parameter in their model to simulate this.

It is possible to also include diffuser stall in a similar fashion. For a vaneless diffuser we would argue that the shroud-side area of the impeller and diffuser is blocked due to recirculation. Therefore, we could create a similar blockage formula that involves the diffuser inlet flow angle and a critical angle at which recirculation occurs. We would also be able to account for impeller backsweep in this stall model by considering its effect on the diffuser inlet angle.

If instead we were working on a vaned diffuser, we would use an area blockage argument that follows very closely to that of the impeller using the inlet diffuser flow angle and the angle of the vanes.

NUMERICAL IMPLEMENTATION AND RESULTS

In order to implement this numerically, it is possible to reduce each system of ODEs for the impeller and diffuser into just one ODE for density, ρ. After rearranging, we get

$$\frac{\partial \rho}{\partial r} = \frac{-\rho q^2 \left(\frac{1}{r} + \frac{1}{h}\frac{\partial h}{\partial r}\right) - \Omega^2 r^3 h^2 \rho^3 + \gamma f \rho q^2 \left(\frac{n_b}{2\pi r} + \frac{1}{h}\right)}{\left(\frac{\gamma+1}{2}\right) q^2 - (\gamma - 1)\left(\frac{\Omega^2 r^2}{2} + E_I\right) r^2 h^2 \rho^2}, \tag{51}$$

for the impeller and

$$\frac{\partial \rho}{\partial r} = \frac{-\frac{\rho q^2}{r} - r^2 h^2 \rho^3 \left(\gamma \frac{u_\theta^2}{r} + (\gamma - 1) u_\theta \frac{\partial u_\theta}{\partial r}\right) + \gamma \frac{f}{h} \rho q^2}{\left(\frac{\gamma+1}{2}\right) q^2 + (\gamma - 1)\left(\frac{u_\theta^2}{2} - E_D\right) r^2 h^2 \rho^2}, \tag{52}$$

for the diffuser, where

$$rh\rho u_r = q = \text{const.}, \tag{53}$$

$$\frac{u_r^2}{2} + \frac{\gamma}{\gamma - 1}\frac{p}{\rho} - \frac{\Omega^2 r^2}{2} = E_I = \text{const.}, \tag{54}$$

$$\frac{u_r^2}{2} + \frac{u_\theta^2}{2} + \frac{\gamma}{\gamma - 1}\frac{p}{\rho} = E_D = \text{const.}, \tag{55}$$

$$u_\theta = \frac{\Omega r_{\text{tip}}^2}{r} e^{-\frac{f}{h}\left(r - r_{\text{tip}}\right)}. \tag{56}$$

Observing that

$$q = \frac{\dot{m}}{\theta}, \tag{57}$$

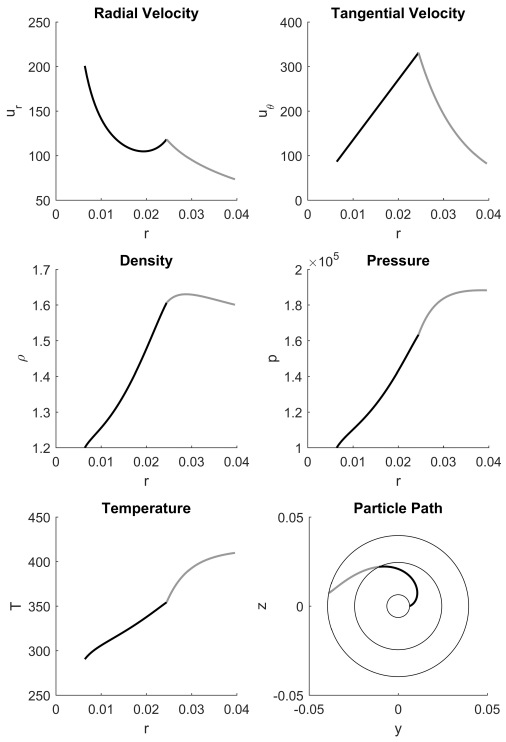

Fig. 3. SIMULATED GAS PROPERTIES AS AIR PASSES THROUGH A SMALL COMPRESSOR. THIS SHOWS A STABLE OPERATING POINT, WITH THE IMPELLER SPINNING AT 130 krpm AND A MASS FLOW OF 0.1 kg/s. ALL BLACK LINES INDICATE THE FLOW IS IN THE IMPELLER AND ALL GREY LINES INDICATE THE FLOW IS IN THE DIFFUSER.

where θ is defined as before to take into account inlet stalling, we can write

$$q = \begin{cases} \frac{\dot{m}}{2\pi}\left(1+\alpha\left(1-\frac{\tan\beta_B}{\tan\beta}\right)^2\right) & \beta > \beta_B \\ \frac{\dot{m}}{2\pi} & \text{otherwise.} \end{cases} \tag{58}$$

These ODEs can be solved quickly in MATLAB using `ode45` to simulate flow through the compressor in steady state. Figure 3 shows how the properties of the flow change as it passes through the impeller and diffuser.

We observe that the tangential velocity is increasing in the impeller with radial distance due to the fixed impeller angular speed. However, in the diffuser there is no forced rotation and the tangential velocity decreases due to diffusion and frictional forces.

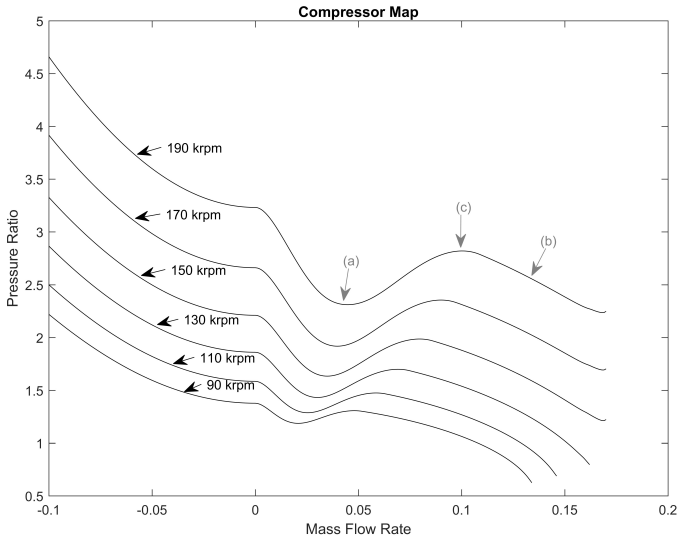

Fig. 4. SIMULATED STATIC PRESSURE COMPRESSOR CHARACTERISTICS FOR SIX DIFFERENT IMPELLER SPEEDS, LABELLED ON EACH LINE IN krpm. THE POINTS (a) AND (b) CORRESPOND TO LOCATIONS WHERE STALLING AND FRICTION ARE DOMINANT EFFECTS RESPECTIVELY. THE POINT (c) IDENTIFIES THE LOCAL MAXIMUM THAT IS USED IN FIG. 9

The radial velocity is generally decreasing due to diffusion and friction. In the impeller there is a balance between diffusion, as the channel is increasing in area, and centrifugal forces, which accelerate the flow radially. The centrifugal forces dominate at large tangential velocities, which is why the velocity begins to increase near the impeller exit.

Since we have diffusion in both the impeller and diffuser, the pressure and density rise occurs in both components. The temperature also rises throughout the compressor because of friction. In the diffuser friction is acting against both the radial and tangential component of velocity, whereas in the impeller the tangential velocity is dictated by the impeller rotation and so friction only acts against the radial velocity. Therefore we see a sharper rise in temperature in the diffuser.

The particle path shows us that the flow is travelling in an Archimedean spiral in the impeller due to the radial blades and the forced rotation. This turns into an approximately logarithmic spiral in the diffuser. If there was no friction in the diffuser, we would have a true logarithmic spiral as the path would be that of a free vortex.

Running this simulation for multiple impeller speeds and mass flows and plotting the outlet static pressure produces compressor characteristics, as seen in Fig. 4. Notice that because we also know the outlet density and velocity, we can compute the total pressure characteristic (and hence the total-to-total pressure ratio at each point).

By varying factors within the simulation, it is easy to discover why we get this cubic-like shape. The local minimum at low mass flows (Fig. 4 point (a)) is caused by stalling in the impeller and changes with values of the stall parameter α. The negative slope to the right of the local maximum (Fig. 4 point (b)) is due to friction and changes with the value of the friction factor f. Finally, in reversed flow the compressor acts as a restrictor, and so the characteristic has a negative slope because it follows a shape similar to that of an orifice.

Parameter fitting

In order for the model to be predictive, relationships for the two parameters in the model, f and α, need to be determined. These relationships must only depend on the known model variables, such as mass flow or impeller speed.

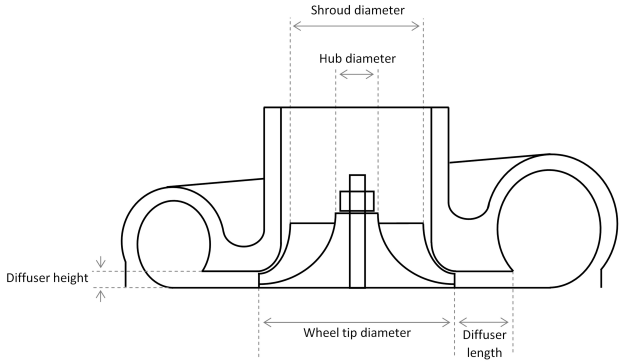

Fig. 5. DIAGRAM INDICATING THE DIMENSIONS GIVEN IN TABLE 1.

Table 1. GEOMETRIC DETAILS OF THE COMPRESSORS USED FOR PARAMETER FITTING AND VALIDATION. FIGURE 5 CAN BE REFERRED TO FOR EXPLANATION OF THE DIMENSIONS.

	Dataset A	Dataset B
Number of blades	$6+6$	$6+6$
Hub diameter	12.8 mm	10 mm
Shroud diameter	33.5 mm	29.6 mm
Wheel tip diameter	49 mm	40 mm
Diffuser height	3.4 mm	3 mm
Diffuser length	15.1 mm	15.7 mm
Diffuser area ratio	1.6	1.8

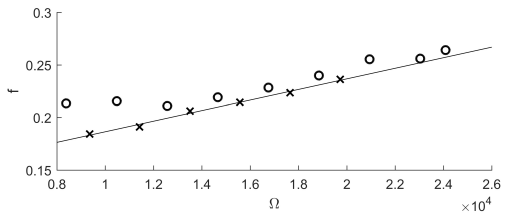

Fig. 6. LINE INDICATING THE DISCOVERED LINEAR RELATIONSHIP BETWEEN FRICTION PARAMETER, f, AND IMPELLER SPEED, Ω. THE CROSSES ARE FOR THE COMPRESSOR IN DATASET A, AND THE CIRCLES ARE FOR THE COMPRESSOR IN DATASET B.

We shall demonstrate this process via the use of two datasets; one for finding the relationship, and the other for checking this relationship holds across different compressors. For ease, let's label these datasets as A and B. Each dataset is from an experimental study performed on the gas stand at the University of Bath, and consists of a compressor map, detailing the total-to-total pressure ratio at different mass flows and impeller speeds, and surge data, including the peak static pressure oscillation amplitude for each impeller speed. Table 1 gives geometric details of the compressors associated with each dataset, where Fig. 5 can be used for reference.

Consider the friction parameter, f. Using dataset A, we can find a value for f at each impeller speed by performing a least squares fit from the model line to the compressor map data. For this, we are careful to only use the points in the dataset that are truly steady (i.e. show no form of oscillation above the normal noise level in the data) because our compressor characteristics only output steady-state compressor behaviour. This provided us with a linear relationship between the friction parameter and impeller speed given by

$$f = 0.14 + 5 \times 10^{-6}\Omega \tag{59}$$

where Ω is in radians per second. To validate this relationship, we perform a least squares fit for each speed line in dataset B (again using steady points only). Figure 6 shows the linear relationship found from dataset A (crosses) alongside the desired values of f for dataset B (circles). Dataset B also appears to share the linear relationship, but the fit would be better if there was a minor shift to the intercept. Implementing this shift has no visible effect on the resulting characteristics, so the original relationship is used.

In reality, there would be 3D flow effects, such as eddy currents, that would add to the losses in the compressor at higher rotational speeds. These features cannot be captured by this 1D model, and so are

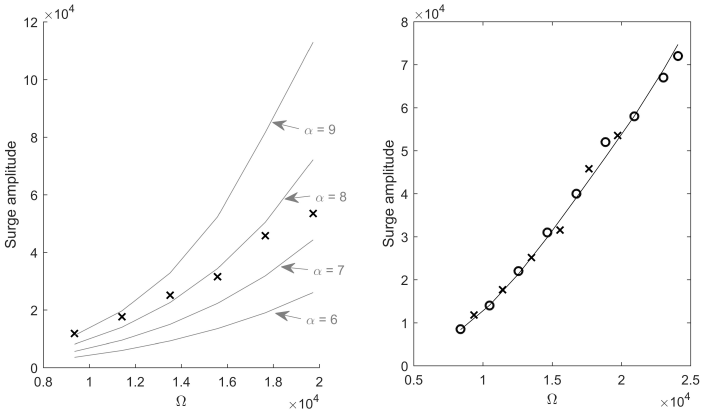

Fig. 7. LEFT: COMPUTED RELATIONSHIP BETWEEN IMPELLER SPEED AND AMPLITUDE OF SURGE OSCILLATIONS IN THE MODEL FOR DIFFERENT VALUES OF THE STALLING PARAMETER, α. THE AMPLITUDE DATA FROM DATASET A IS SHOWN AS CROSSES FOR COMPARISON. RIGHT: RESULT WHEN USING THE DISCOVERED RELATIONSHIP FOR STALLING PARAMETER α. THE CROSSES ARE FROM DATASET A, AND THE CIRCLES ARE FROM DATASET B.

being encompassed into the friction parameter via this relationship.

For determining the stalling parameter α we can look at the peak static pressure amplitude observed while operating at surge for each speed line in dataset A. The left hand side graph in Fig. 7 shows how the value of α impacts the relationship between the observed peak surge amplitude and the impeller speed for the model. Exploiting this we can determine that

$$\alpha = 10.3 - 1.5 \times 10^{-4}\Omega. \tag{60}$$

The right hand side graph in Fig. 7 shows the resulting trend in the impeller speed - surge amplitude relationship, along with the surge amplitude data for dataset B. This fit is very good across the different compressors.

QUASI-STEADY MODEL

We can now use the compressor characteristics developed above by creating a model for the flow between the compressor and a throttle valve. Ideally, we should end up with a system of ODEs similar to that of Eqns. 1 & 2.

The compressors corresponding to datasets A and B were both tested on a rig that had a pipe without a plenum connecting it to the throttle value. Therefore, using the equations of mass and momentum in the

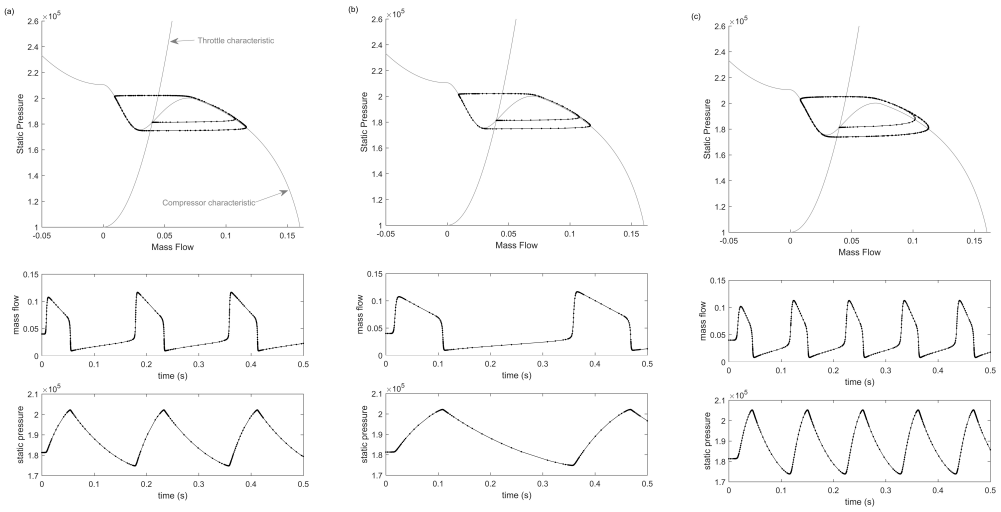

Fig. 8. THREE SIMULATED CASES: (a) 3m LENGTH OF 3in DIAMETER PIPE, (b) 6m LENGTH OF 3in DIAMETER PIPE and (c) 3m LENGTH OF 1.5in DIAMETER PIPE. FOR EACH CASE THE TOP GRAPH IS A SIMULATED SURGE LIMIT CYCLE IN THE MASS FLOW-STATIC PRESSURE PLANE, WITH THE COMPRESSOR AND THROTTLE CHARACTERISTICS IDENTIFIED IN GREY, AND THE BOTTOM GRAPH IS THE CORRESPONDING SIMULATED PRESSURE AND MASS FLOW OSCILLATIONS.

inertial frame (Eqns. 5 & 6 with $\Omega = 0$), along with the assumption of an isentropic gas,

$$p = \kappa \rho^{\gamma}, \tag{61}$$

allows us to obtain the following system of equations for the flow in the compression system:

$$\frac{d\dot{m}}{dt} = \frac{A}{L}(p_c(\dot{m}) - p) + \frac{\kappa^{\frac{1}{\gamma}}}{AL}\left(\frac{\dot{m}^2}{p_c(\dot{m})^{\frac{1}{\gamma}}} - \frac{\dot{m}_T(p)^2}{p^{\frac{1}{\gamma}}}\right), \tag{62}$$

$$\frac{dp}{dt} = \frac{\gamma \kappa^{\frac{1}{\gamma}}}{AL} p^{\frac{\gamma-1}{\gamma}}(\dot{m} - \dot{m}_T(p)), \tag{63}$$

where $\dot{m}_T$ is the throttle characteristic and p_c is the steady-state compressor characteristic developed within this paper.

For the throttle characteristic we can use

$$\dot{m}_T^2(p) = \frac{2\gamma}{\gamma - 1}\left(\frac{\lambda^2 A^2 \rho \rho_{\text{amb}}}{\lambda^2 \rho_{\text{amb}}^2 - \rho^2}\right)(\rho p_{\text{amb}} - \rho_{\text{amb}} p), \tag{64}$$

where λ is the fraction the throttle is open. This has come from the steady-state forms of conservation of mass and energy (Eqns. 5 & 7) applied to two points: one before the throttle, which has unknown density, pressure and mass flow values, and one after the throttle, which is assumed to be at ambient conditions.

This system can then be solved numerically to identify the time-dependent behaviour of the compression system. The operating point of the system is the intersection of the throttle characteristic $\dot{m}_T$ and the compressor characteristic p_c in the mass flow - static pressure plane. There are two observed behaviours with this system.

The first is steady behaviour where pressure and mass flow remain constant with time. The second is oscillating behaviour as shown in Fig. 8(a). In this case, we get a trajectory in time that tracks the negatively sloped regions of the compressor characteristic closely, travelling quickly between them. It causes oscillations in mass flow and pressure of about 6 Hz, which is good as surge typically is a low frequency phenomena.

The dynamics of this oscillating state depends on the geometry of the pipework between the compressor and the throttle. Figures 8(b) and 8(c) show an example of what happens when the length, L, and the cross-sectional area, A, of the pipe change. The pipe length influences the frequency of the simulated oscillations because if L increases the frequency decreases (and vice versa). The cross-sectional area has a more complex effect on the dynamics. It influences the frequency in the same way as L (larger area results in a decreased frequency and vice versa) but it has the additional effect that as A becomes small the shape of the limit cycle becomes smoother and doesn't track the compressor characteristic as close.

What is clear from all the limit cycles in Fig. 8 is that the shape of the compressor characteristic is key to the dynamics. Therefore, changing things like the inlet blade angle will alter the location of the point in which we see oscillations, i.e. our surge line. It also means that as the shape of the compressor characteristic becomes more accurate by, say, adding in a diffuser stall, we will be able to capture more of the surge dynamics.

It is good that our model can capture changes in the simulated surge dynamics for different pipe geometries and compressor characteristics because it means that it is able to simulate the testing of different compressors on different test rigs.

Model validation

In order to evaluate our model more quantitatively, we can run this quasi-steady model at different throttle openings and compute a time average of the pressure and mass flows. This can be used to produce

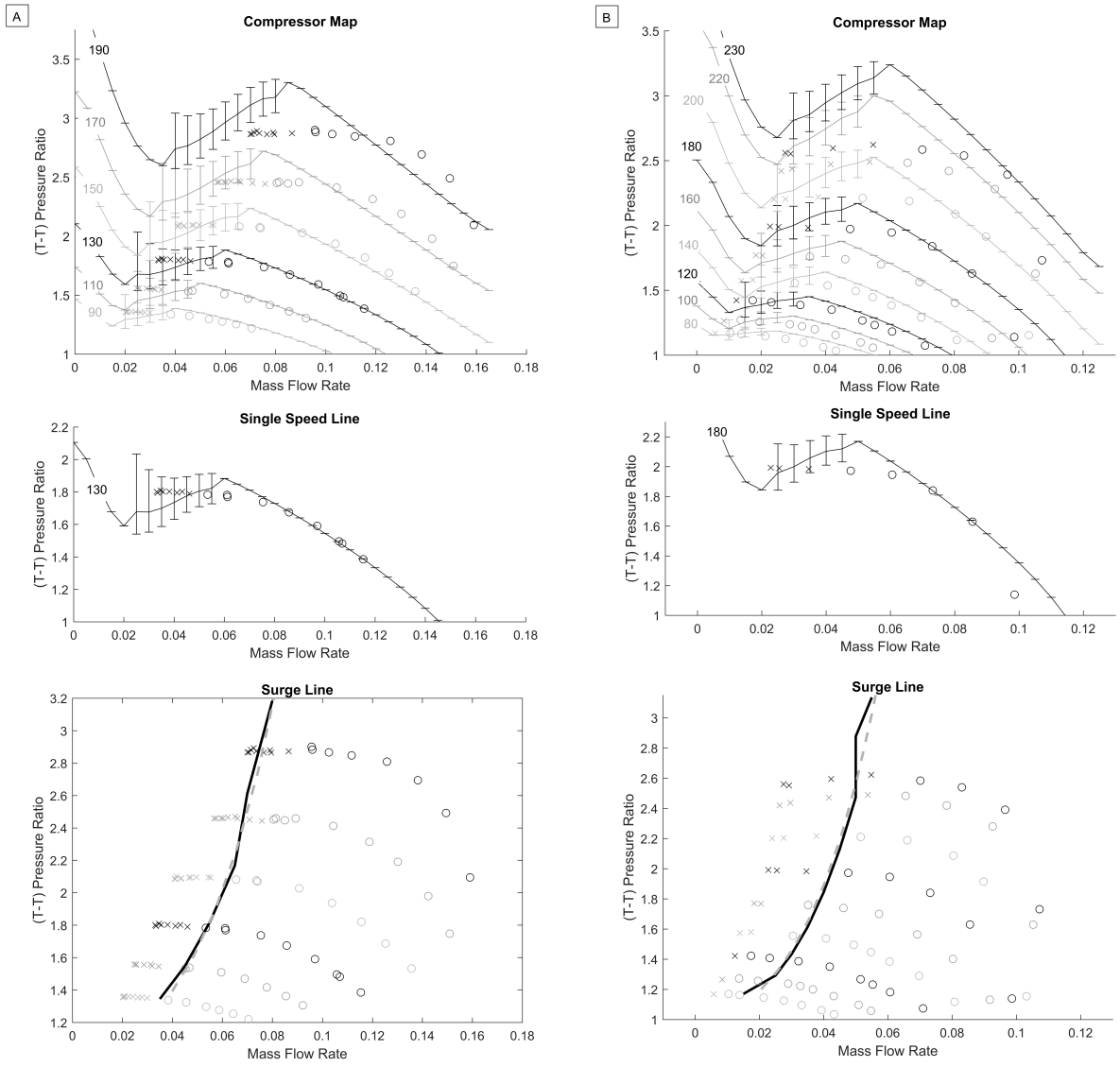

Fig. 9. COMPARISON BETWEEN THE SIMULATED TOTAL-TO-TOTAL COMPRESSOR MAP AND THE DATA FOR DATASETS A AND B. THE SIMULATED MAP HAS BEEN PLOTTED AS LINES WITH BARS SHOWING THE MAX AND MIN SIMULATED VALUES. THE DATA IS SHOWN WITH CIRCLES IF IT IS STEADY AND CROSSES IF IT SHOWED OSCILLATIONS LARGER THAN THE AVERAGE NOISE LEVEL. THE SPEED IN krpm IS INDICATED ON EACH LINE. FOR CLARITY, A SINGLE SPEED LINE FROM THE MIDDLE OF THE MAP IS SHOWN SEPARATELY BELOW. FINALLY, SITUATED AT THE BOTTOM, THE SIMULATED SURGE LINE IS SHOWN (IN SOLID BLACK) IN COMPARISON TO THE DATA. THE DASHED GREY LINE SHOWS THE LOCATION OF THE LOCAL MAXIMUM OF THE COMPRESSOR CHARACTERISTICS (FIG. 4 POINT (c)) FOR COMPARISON.

a time-averaged compressor map, which is essentially what we get through testing. Figure 9 shows this time-averaged map with experimental data points for both datasets A and B.

We have chosen to classify the data into two categories: those that only show oscillations at the average noise level (which changes from about 100Pa to 1000Pa as the impeller speed increases) are considered

steady, and those that show oscillations greater than that are considered unsteady. In Fig.9 we have plotted the steady data as circles and the unsteady data as crosses.

For the simulated compressor map, we have plotted bars that identify the range of values seen when computing the time-average solution. From this we can see a clear line that indicates the onset of oscillations in our model. We call this the simulated surge line and have shown this with comparison to the data underneath each map.

Our simulated surge line is very close to the local maximum of the compressor characteristics (see Fig. 4 point (c)), which is shown with a grey dashed line in the figure. Since the gradient of the characteristic (and hence the location of local maximum and minimum) is determined by the impeller inlet stall, we can deduce that this stall is triggering our simulated compressor into surge.

We can also see that our simulated surge line is close to the point in the data where it switches from steady behaviour to mild oscillation. It appears to predict an earlier surge onset for lower impeller speeds, but it is possible that this is due to the fact that distinguishing between noise and mild oscillations is difficult for these points.

At high speeds our surge line is within the region of mild oscillation (or mild surge) and, for compressor A, is getting close to the deep surge limit (the left-most data point). This suggests that the trigger for mild surge at these points is likely to be something other than impeller inlet stall, and that it is this in combination with the impeller inlet stall that causes deep surge.

The simulated amplitude of the oscillations is increasing as mass flow decreases, which is very promising as in experiments the oscillations typically grow towards the deep surge limit (where testing is stopped to prevent damage to the compressor). However, as mass flow is reduced, there becomes a point in our simulated map that the oscillations stop and the flow becomes stable again. This may indeed be true because Koff and Greitzer [20] found during their experimental study of the compressor map that the flow can become stable again close to shut-off. However, we have some unsteady data points that lie in this part of our curves, so our region of stability is currently larger than is observed experimentally.

When examining the fit of the data to the simulated average total-to-total pressure ratio curves, we can see that for speeds under 200krpm the points follow the steady portion of the curve closely, and for speeds under 180krpm the time-averaged unsteady points are also a reasonable fit. From the single speed line plots it is clear to see that, as mass flow decreases, our model predicts steady flow behaviour with an increasing pressure ratio until the simulated surge line, and unsteady flow behaviour with a decreasing average pressure ratio after that point. When the data approaches the surge line it seems to flatten out

instead, but usually remains within the simulated range of oscillation.

From the single speed line for dataset B, we can see that the model is not always able to simulate the pressure ratios for high mass flows. This is because at high mass flows we approach the choked flow region, and the Mach number for the flow increases towards one. Our model doesn't include any form of shock loss that would occur as the flow approaches the speed of sound, and so doesn't contain all the physics required to capture the choked flow behaviour.

Above speeds of 200krpm the fit is not as good, meaning that our model is missing some important physical dynamics for the higher impeller speeds. Diffuser stall is a phenomenon that is usually triggered first at higher impeller speeds, therefore incorporating this into the model is expected to improve the fit and surge dynamics at these higher speeds.

Overall, this model has been able to predict a surge line for a compressor by only considering its geometry. There are inaccuracies in the model but we have made a choice to compromise on accuracy for the sake of having a predictive model, and these inaccuracies can be improved upon as more dynamics are added.

SUMMARY AND CONCLUSIONS

A new method for producing compressor characteristics has been presented, updating the work on low-dimensional surge models developed during the 1970s. An original steady-state compressor model was developed from the mass, momentum and energy conservation laws, along with two factors to model friction and stalling. Creating the model this way allowed for insight into various features observed in a compressor characteristic. For example, stalling creates a local minimum and maximum in low forward mass flows. Since the location of this feature correlates to the location of the surge line in our model, we were able to identify impeller inlet stall as a route into surge.

The model equations were reduced and simplified to form ODEs that are quick to solve. If full 3D CFD was used to model flow in a compressor near surge, this highly complex problem becomes very computationally expensive. Low-dimensional surge models are a viable alternative because the need for quick evaluations outweighs the need for high accuracy, and so it is vital that this speed of computation is maintained.

Relationships for the friction parameter and stalling parameter with impeller speed were found by comparison to test data. These relationships hold across multiple compressor geometries, allowing the model to be fully deterministic. Therefore, the model has the ability to be a predictive tool for surge limits of new

compressor designs because it only needs geometric measurements as inputs.

The model showed promising results when compared to compressor map data, and is able to capture reasonably realistic surge frequencies when included in a low-dimensional surge model. It is able to identify when oscillations in mass flow and pressure are likely to appear, and is able to capture a growing amplitude in oscillations as the mass flow is further reduced.

Further work is planned to include diffuser recirculation or stall into this model. It is generally agreed that diffuser stall can trigger surge at higher impeller speeds, which will hopefully improve the accuracy of the model's surge limit.

ACKNOWLEDGEMENTS

The authors are grateful to Tomasz Duda, Stefan Tuechler, and Zheng Liu, who provided the geometry, compressor map and surge amplitude data within this paper.

Katherine Powers is supported by a scholarship from the EPSRC Centre for Doctoral Training in Statistical Applied Mathematics at Bath (SAMBa), under the project EP/L015684/1.

NOMENCLATURE

A Cross-sectional area

B Greitzer's parameter

c_v Specific heat at constant volume

E Specific energy

F Friction

f Friction factor

$\mathbf{g}$ Acceleration due to gravity

h Channel height

L Length

$\dot{m}$ Mass flow

n_b Number of impeller blades

p Static pressure

q Mass flow per radian

$\dot{Q}$ Specific heat energy

R Specific gas constant

r Radius

S Surface area

T Temperature

U Specific internal energy

u Velocity

α Stalling factor

β Flow angle

β_B Blade angle

γ Specific heat ratio

κ Isentropic constant

λ Fraction throttle is open

ξ_T Throttle parameter

ρ Density

τ Stress

Φ Nondimensional mass flow

Ψ Nondimensional pressure

Ω Angular velocity

Subscripts:

amb Ambient

c Compressor

D Diffuser

I Impeller

r Radial direction

T Throttle

tip Impeller tip

x Axial direction

θ Tangential direction

Acronyms:

CFD Computational fluid dynamics

ODE Ordinary differential equation

Other:

`ode45` Numerical ODE solver within MATLAB

REFERENCES

[1] Rasmussen, P. C., and Kurz, R., 2009. "Centrifugal compressor applications-upstream and mid-stream.". In Proceedings of the 38th Turbomachinery Symposium, Texas A&M University. Turbomachinery Laboratories.

[2] Macdougal, I., and Elder, R., 1983. "Simulation of centrifugal compressor transient performance for process plant applications". *Journal of engineering for power,* **105**(4), pp. 885–890.

[3] Stone, R., 2012. *Introduction to internal combustion engines*, 4 ed. Palgrave MacMillan.

[4] Watson, N., and Janota, M. S., 1982. *Turbocharging: The internal combustion engine*. MacMillan.

[5] Pampreen, R. C., 1993. *Compressor surge and stall*. Concepts Eti.

[6] Fink, D. A., Cumpsty, N. A., and Greitzer, E. M., 1992. "Surge dynamics in a free-spool centrifugal compressor system". *Journal of Turbomachinery,* **114**, pp. 321– 332.

[7] De Jager, B., 1995. "Rotating stall and surge control: A survey". In Proceedings of the 34th IEEE Conference on Decision and Control, Vol. 2, IEEE, pp. 1857–1862.

[8] Longley, J. P., 1994. "A review of nonsteady flow models for compressor stability". *Journal of Turbomachinery,* **116**, pp. 202–215.

[9] Stenning, A. H., 1980. "Rotating stall and surge". *Journal of Fluids Engineering,* **102**(1), pp. 14–20.

[10] Linfield, K. W., and Mudry, R. G., 2008. "Pros and cons of cfd and physical flow modeling". *Airflow Sciences Corporation*.

[11] Cozzi, L., Rubechini, F., Marconcini, M., Arnone, A., Astrua, P., Schneider, A., and Silingardi, A., 2017. "Facing the challenges in cfd modelling of multistage axial compressors". In ASME Turbo Expo 2017: Turbomachinery Technical Conference and Exposition, American Society of Mechanical Engineers.

[12] Arnulfi, G. L., Giannattasio, P., Giusto, C., Massardo, A. F., Micheli, D., and Pinamonti, P., 1999. "Multistage centrifugal compressor surge analysis: Part II - Numerical simulation and dynamic control parameters evaluation". *Journal of Turbomachinery,* **121**(2), pp. 312–320.

[13] Van Helvoirt, J., de Jager, B., Steinbuch, M., and Smeulers, J., 2004. "Stability parameter identification for a centrifugal compression system". In 43rd IEEE Conference on Decision and Control, Vol. 4, IEEE,

pp. 3400–3405.

[14] Mizuki, S., Asaga, Y., Ono, Y., and Tsujita, H., 2006. "Investigation of surge behavior in a micro centrifugal compressor". *Journal of Thermal Science,* **15**(2), pp. 97–102.

[15] Tamaki, H., 2008. "Effect of piping systems on surge in centrifugal compressors". *Journal of Mechanical Science and Technology,* **22**(10), pp. 1857–1863.

[16] Galindo, J., Arnau, F., Tiseira, A., and Piqueras, P., 2010. "Solution of the turbocompressor boundary condition for one-dimensional gas-dynamic codes". *Mathematical and Computer Modelling,* **52**, pp. 1288–1297.

[17] Torregrosa, A., Arnau, F., Piqueras, P., Reyes-Belmonte, M., Knutsson, M., and Lennblad, J., 2012. Acoustic one-dimensional compressor model for integration in a gas-dynamic code. Tech. rep.

[18] Greitzer, E. M., 1976. "Surge and rotating stall in axial flow compressors - Part I: Theoretical compression system model". *Journal of Engineering for Power,* **98**(2), pp. 190–198.

[19] Hős, C., Champneys, A., and Kullmann, L., 2003. "Bifurcation analysis of surge and rotating stall in the Moore–Greitzer compression system". *IMA Journal of Applied Mathematics,* **68**(2), pp. 205–228.

[20] Koff, S. G., and Greitzer, E. M., 1984. "Stalled flow performance for axial compressors: I - Axisymmetric characteristic". In 29th International Gas Turbine Conference and Exhibit, Vol. 1, American Society of Mechanical Engineers.

[21] Galindo, J., Serrano, J. R., Climent, H., and Tiseira, A., 2008. "Experiments and modelling of surge in small centrifugal compressor for automotive engines". *Experimental Thermal and Fluid Science,* **32**(3), pp. 818–826.

[22] Moore, F. K., and Greitzer, E. M., 1986. "A theory of post-stall transients in axial compression systems: Part I - Development of equations". *Journal of Engineering for Gas Turbines and Power,* **108**(1), pp. 68–76.

[23] Zagorowska, M., and Thornhill, N. F., 2017. "Compressor map approximation using chebyshev polynomials". *25th Mediterranean Conference on Control and Automation (MED)*, pp. 864–869.

[24] Li, X., Yang, C., Wang, Y., and Wang, H., 2018. "A prediction model of compressor with variable-geometry diffuser based on elliptic equation and partial least squares". *Royal Society open science,* **5**.

[25] Elder, R. L., and Gill, M. E., 1985. "A discussion of the factors affecting surge in centrifugal compressors". *Journal of Engineering for Gas Turbines and Power,* **107**, pp. 499–506.

[26] Martin, G., Talon, V., Higelin, P., Charlet, A., and Caillol, C., 2009. "Implementing turbomachin-

ery physics into data map-based turbocharger models". *SAE International Journal of Engines,* **2**(1), pp. 211–229.

[27] Japikse, D., 1996. *Centrifugal compressor design and performance*, Vol. 2. Concepts Eti, White River Junction, VT.

[28] Velásquez, E. I. G., 2017. "Determination of a suitable set of loss models for centrifugal compressor performance prediction". *Chinese Journal of Aeronautics,* **30**, pp. 1644–1650.

[29] Oh, H. W., Yoon, E. S., and Chung, M. K., 1997. "An optimum set of loss models for performance prediction of centrifugal compressors". *Proceedings of the Institution of Mechanical Engineers, Part A: Journal of Power and Energy,* **211**(4), pp. 331–338.

[30] Gong, X., and Chen, R., 2014. "Total pressure loss mechanism of centrifugal compressors". *Journal of Mechanical Engineering Research,* **4**(2), pp. 45–59.

[31] Burr, K. P., Akylas, T. R., and Mei, C. C. Chapter 2: Two-dimensional laminar boundary layers. `http://web.mit.edu/fluids-modules/www/highspeed_flows/ver2/bl_Chap2.pdf`. [Online], Accessed 27/03/2017.

[32] Winterbone, D. E., and Pearson, R. J., 2000. *Theory of engine manifold design: Wave action methods for IC engines*. Professional Engineering Publishing.

[33] Day, I. J., Greitzer, E. M., and Cumpsty, N. A., 1978. "Prediction of compressor performance in rotating stall". *Journal of Engineering for Power,* **100**(1), pp. 1–12.